

Kinetic Sunyaev-Zeldovich effect from galaxy cluster rotation

Nikolas Karl Pässler

Bachelorarbeit in Physik
angefertigt im Physikalischen Institut

vorgelegt der
Mathematisch-Naturwissenschaftlichen Fakultät
der
Rheinischen Friedrich-Wilhelms-Universität
Bonn

April 2021

Ich versichere, dass ich diese Arbeit selbstständig verfasst und keine anderen als die angegebenen Quellen und Hilfsmittel benutzt sowie die Zitate kenntlich gemacht habe.

Bonn,
Datum Unterschrift

1. Gutachter: Dr. Kaustuv Basu
2. Gutachter: Prof. Dr. Frank Bertoldi

Contents

1	Introduction	1
1.1	Cosmic microwave background	1
1.2	Galaxy clusters	2
1.3	The Sunyaev-Zeldovich effect	2
1.3.1	Compton effect	3
1.3.2	Optical depth	3
1.3.3	Electron density	3
1.3.4	Intensity change (kSZE)	4
1.3.5	Polarization	4
2	Calculation	7
2.1	Parameterization	7
2.2	Optical depth	8
2.3	Rotational velocity	8
2.4	Relative intensity change	10
2.4.1	Temperature change	11
2.5	Polarization	12
2.5.1	Average polarization of multiple galaxy clusters	15
3	Conclusion and Outlook	19
4	Appendix	21
4.1	Software	21
4.2	Temperature change figure	21
4.3	Polarization figures	22
	List of Figures	27

CHAPTER 1

Introduction

In this thesis will the kinetic *Sunyaev-Zeldovich* effect be discussed. More precisely, the intensity or temperature change, respectively and polarization of the *cosmic microwave background* (CMB) due to internal gas movements in galaxy clusters will be discussed.

The Sunyaev-Zeldovich effect occurs because of Compton and inverse Compton scattering of the CMB-photons on high energetic electrons in galaxy clusters which leads to distortions of the CMB. One distinguishes three types of this effect. The *thermal* effect is obtained by scattering off the thermal motion in the electron gas and the *kinetic* effect is caused by scattering off electrons with high energies owing to bulk motion. The rotational motion of galaxy clusters provides such a bulk motion of electrons and thus results in a distortion of the CMB. Besides the thermal and kinetic Sunyaev-Zeldovich effect also arises polarization of the CMB because of scattering on bulk moving electrons.

This thesis focuses on the kinetic Sunyaev-Zeldovich and the polarizing effect of the CMB. As one will see in this thesis, the effects are not that strong, in particular the polarizing effect. This makes observation difficult. Therefore I will also determine the average polarization of several galaxy clusters by stacking them to gain a possibility of observation.

1.1 Cosmic microwave background

The Cosmic microwave background is a relict of the beginning of the universe when it was a hot plasma of matter and radiation coupled together. It is a precisely shaped black body radiation [1] that is almost isotropic after subtraction of the “solar” and “orbital dipole”. The “solar dipole” is induced by the motion of the solar system with respect to the CMB. The “orbital center” is induced by the motion of the observer in the solar system [2].

The temperature of the CMB spectrum is $T_{\text{CMB}} = (2.725 \pm 0.001)$ K [3]. Planck’s Law [4] describes the intensity of the black body radiation with the temperature T_{CMB} :

$$I_\nu = \frac{2h\nu^3}{c^2} \frac{1}{e^{\frac{h\nu}{k_B T_{\text{CMB}}}} - 1} \quad (1.1)$$

The CMB intensity peaks at $\nu \approx 160.2$ GHz [3].

1.2 Galaxy clusters

Galaxy clusters are large-scale gravitational bound structures comprising tens to thousands of galaxies. Whereas the radii (galaxy surface density drops to $\sim 1\%$) of these structures lay at $(1 - 2)\text{Mpc}$. The core radii, where the density drops to half the maximum, are at about $(0.1 - 0.25)\text{Mpc}$ [5, 6].

The intergalactic space of these structures is filled with a hot gas, called intracluster medium (ICM). The electron density in the ICM of galaxy clusters was traditionally described by the isothermal β -model [7]. In Vikhlinin et al. (2006) [8] a better fitted model was proposed which was simplified and analyzed in Baldi et al. (2018) [9] on a subset of objects from the MUSIC¹ hydrodynamical N-body simulation project [10] (see section 1.3.3).

Overall, the rotational dynamics of galaxy structures are not well studied. It is suggested, that the gas in galaxy clusters follows the dark matter motion, which has a universal momentum profile of a solid-body rotation. This saturates, though, for large values [11], with circular velocities (velocity at viral radius r_{vir}^2) of the order of $\sim 1500 \text{ km s}^{-1}$ ($v_{\text{circ}} = \sqrt{GM_{\text{vir}}/r_{\text{vir}}}^3$ [9]), which leads to velocities of the order of a few to a few ten km s^{-1} at the core radius [11, 12]. This profile will be referred hereafter as VP1.

In a more sophisticated work by Baldi et al. (2016) [13] where radial velocity profiles of simulated galaxy clusters were examined. Three differential velocity profiles were used, to describe the rotational velocity of the ICM and dark matter in clusters. All of them have a steep increase of velocity in the center followed by an outward decrease after a velocity peak and only differ in the steepness of the increase and the deepness of the decrease (see figure 2.5). They found their “vp2b” model (see equation 2.6) to fit best a set of MUSIC objects.

1.3 The Sunyaev-Zeldovich effect

The *Sunyaev-Zeldovich effect* (SZE) describes the distortion of the CMB by Compton scattering of low-energy photons on high-energy electrons in the ICM. It is divided into three different types. The thermal SZE (thSZE) is caused by inverse Compton scattering of CMB photons of electrons with high energy because of the hot temperature of the ICM [14, Zeldovich & Sunyaev, 1969]. The kinetic SZE (kSZE) arises from photons scattering of electrons because of their bulk motion [15, Sunyaev & Zeldovich, 1980]. These two effects lead to a shift of the intensity or equivalently the temperature of the CMB. Besides the thSZE and kSZE, the interaction of the CMB photons with the ICM also leads to polarization of the CMB radiation.

In this thesis, I will only examine the kinetic SZE and the polarizing effect of the CMB. While the kSZE only depends on the velocity component parallel to the line of light, the polarizing effect only depends on the perpendicular component. Together, these effects make a valuable tool to investigate the motions of galaxy clusters. As one will see in this thesis, the effects are not strong, in particular the polarizing effect. This makes observation difficult.

To understand the nature of these effects, a brief introduction to the Compton effect, the optical depth, and the electron density in galaxy clusters will be given.

¹ The Marenostrum-MUltiDark SImulations of galaxy Clusters (MUSIC) data set

² The virial radius r_{vir} is the radius where the cluster virializes ($2E_{\text{kin}} = E_{\text{pot}}$, virial theorem) and therefore is gravitational bound

³ The virial mass M_{vir} is the mass inside the viral radius r_{vir}

1.3.1 Compton effect

The *Compton effect* describes the energy decrease of photons by scattering of charged particles (*compton scattering*) such as electrons. The effect is called *inverse*, if the photon energy rises after scattering on a high-energy particle. This effect causes the thermal SZE.

The energy and impulse is preserved as:

$$E_\gamma + E_e = E_{\gamma'} + E_{e'} \quad (1.2)$$

$$\mathbf{p}_\gamma + \mathbf{p}_e = \mathbf{p}_{\gamma'} + \mathbf{p}_{e'} \quad (1.3)$$

Were $E_\gamma, E_{\gamma'}$ is the energy of the photon before and after the scattering. $E_e, E_{e'}$ is the energy of the electron before and after the scattering. The same applies to the impulses \mathbf{p} .

For $\nu_\gamma \ll m_e c^2/h$ the Compton effect is called Thomson scattering with the photon frequency ν_γ , electron mass m_e , speed of light c , and Planck constant h . In this case, the electron energy stays approximately the same. This is the relevant effect for the kSZE and polarization of the CMB.

1.3.2 Optical depth

The Optical depth τ indicates how well a medium allows electromagnetic waves to pass. Therefore the SZE is proportional to the optical depth. It is proportional to the natural logarithm of the transmittance $\tau = -\ln(T)$ and is therefore dimensionless. The *Beer-Lambert law*

$$T = e^{-\int_0^l dz \mu(z)} \quad (1.4)$$

with the attenuation coefficient $\mu(z) = \sigma_T n_e$, leads to the following equation for the optical depth along the line of sight l :

$$d\tau = \sigma_T n_e(l) dl \quad (1.5)$$

Here is σ_T the Thomson cross-section and n_e the electron density.

1.3.3 Electron density

As already stated, the space in galaxy clusters is filled with the intracluster medium. The electron density n_e was sufficiently described by the isothermal β -model [7] for a long time:

$$n_e(r) = n_0 \left[1 + \left(\frac{r}{r_c} \right)^2 \right]^{-\frac{3}{2}\beta} \quad (1.6)$$

with the central density n_0 , the core radius r_c dependent on the radius r . This model was found to be well fitted for galaxy clusters at $\beta \simeq 2/3$.

Now there are better models to describe the density of the electrons in galaxy clusters, like the one proposed in Vikhlinin et al. (2006) [8]. They have modified the β -model to better describe the

electron density at both the center and the outskirts:

$$n_e(r) = n_0 \frac{(r/r_c)^{-\frac{\alpha}{2}}}{\left[1 + (r/r_c)^2\right]^{\frac{3\beta}{2} - \frac{\alpha}{4}}} \frac{1}{\left[1 + (r/r_s)^3\right]^{\frac{\epsilon}{6}}} \quad (1.7)$$

The parameters r_c and r_s are scale radii, whereas r_c is the core radius, n_0 is the central density. α, β , and ϵ are dimensionless parameters controlling the slopes for different radii. In Baldi et al. (2018) [9] this model was fitted for a few MUSIC clusters and thus the parameters $r_c \sim 0.2 \text{ Mpc}$, $r_s \sim 1.7 \text{ Mpc}$, $n_0 \sim 0.02 \text{ cm}^{-3}$, $\alpha \sim 0.6 - 2$, $\beta \sim 0.7$ and $\epsilon \sim 2.5$ determined.

1.3.4 Intensity change (kSZE)

The kSZE is the intensity change due to Thompson scattering by Doppler boosting. It leads to a decrease or increase of the CMB photon energy, depending on whether the scattering electron is moving towards or away from the observer. The energy change only depends on the velocity component parallel to the line of sight of the scattering electron. This effect leads to an intensity change of the CMB, given as [15]:

$$\Delta I_\nu = I_\nu \frac{x \exp(x)}{\exp(x) - 1} \beta_{\parallel} \tau \quad (1.8)$$

With the dimensionless frequency $x = h\nu/k_B T$ where T is the CMB temperature and k_B is the Boltzmann constant. β_{\parallel} is the line-of-sight velocity in units of c and τ is the optical depth. β_{\parallel} is defined as positive for electrons approaching the observer. This leads to the relative intensity change $d \left(\frac{\Delta I_\nu}{I_\nu} \right)$, which is integrated over the optical depth:

$$d \left(\frac{\Delta I_\nu}{I_\nu} \right) = G_\nu \beta_{\parallel} d\tau \quad (1.9)$$

with $G_\nu = \frac{x \exp(x)}{\exp(x) - 1}$.

The rotation of the ICM, with the rotation axis not purely parallel to the line of sight, leads to a movement of the ICM along the line of sight and, therefore, the kSZE. The effect induced in this way is referred to as the rotational kinetic Sunyaev-Zeldovich effect (rkSZE).

Connected via Plank's law, this leads to a temperature change of:

$$d \left(\frac{\Delta T}{T} \right) = \beta_{\parallel} d\tau \quad (1.10)$$

1.3.5 Polarization

Linear polarization arises by Thomson scattering when the incident radiation field has a quadrupole variation. We can assume the CMB is isotropic and unpolarized, but the movement of the electrons through the CMB rest frame leads to a quadrupole component in the intensity in the rest frame of the electron [16].

Polarization can be described by the *Stokes* parameters I, Q, U & V . The degree of circular polarization V is zero for the SZE since Thomson scattering does not produce circular polarization [12]. Q describes the degree of horizontal ($Q = 1$) and vertical ($Q = -1$) linear polarization. U describes the degree of linear polarization at $\pm 45^\circ$ ($U = \pm 1$).

The Stokes parameters for Thomson scattering can then be calculated as [17, 18]:

$$Q = -\frac{1}{10} I_0 G_{\nu, \text{pol}} \beta_{\perp}^2 \cos(2\chi) d\tau \quad (1.11)$$

$$U = -\frac{1}{10} I_0 G_{\nu, \text{pol}} \beta_{\perp}^2 \sin(2\chi) d\tau \quad (1.12)$$

here is $G_{\nu, \text{pol}} = \frac{e^x (e^x + 1)}{2(e^x - 1)^2} x^2$. β_{\perp} is the velocity perpendicular to the line of light, χ the angle between the velocity and the horizontal axis, and I_0 the intensity of the incoming radiation.

The polarization degree P is calculated by

$$P = \frac{\sqrt{Q^2 + U^2}}{I_{\text{tot}}} \quad (1.13)$$

as $V = 0$ and therefore is P equals the linear polarization degree. $I_{\text{tot}} = I_0(1 - \tau) + I_s$ is the total intensity consisting of the initial Intensity, minus the absorption plus the intensity caused by scattering.

CHAPTER 2

Calculation

The kSZE and polarizing effect caused by Thompson scattering is now be calculated for different velocity profiles. Later, the average degree of polarization is also determined for multiple stacked clusters.

The following calculations are all done numerically in python. Therefore, mainly the packages `numpy` and `scipy` where used. The software used to perform the calculations can be found on GitHub – github.com/npaessler/Kinetic-Sunyaev-Zeldovich-effect-from-galaxy-cluster-rotation.

2.1 Parameterization

The optical depth, relative intensity change and polarization parameters are integrate along the line of sight (see e.g. equation (1.5)) therefore are line integrals used.

I use a coordinate system according to figure 2.1, where the line of sight is almost parallel to the y-axis, because of small viewing angles. The x-axis lays horizontally and the z-axis vertically. The line of sight can then be parametrised in conformity with figure 2.2 to:

$$\vec{l}(t) = \begin{pmatrix} \vartheta t \\ t - d \\ \varphi t \end{pmatrix} \quad (2.1)$$

The line integral for a scalar field $f(\vec{l})$ along the curve (resp. line) C is defined as [19]:

$$\int_C f(\vec{l}) \, ds = \int_{t_1}^{t_2} f(\vec{l}(t)) \left| \vec{l}'(t) \right| \, dt \quad (2.2)$$

where $\vec{l}(t)$ is any bijective parametrization. In case of the line of sight equation (2.1)

For a vector field $\vec{f}(l)$ the line integral is defined as [19]:

$$\int_C \vec{f}(\vec{l}) \, d\vec{l} = \int_{t_1}^{t_2} \vec{F}(\vec{l}(t)) \cdot \vec{l}'(t) \, dt \quad (2.3)$$

where $\vec{F}' = \vec{f}$.

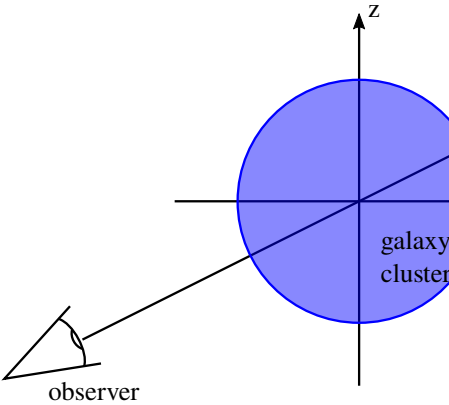


Figure 2.1: Coordinate system

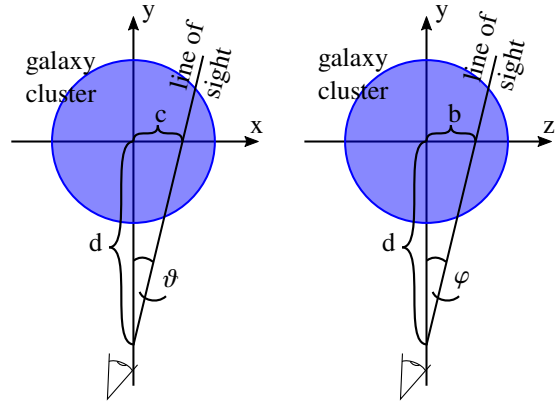


Figure 2.2: Line of sight parametrization

To integrate only from edge to edge of the galaxy cluster one has to find the limits (t_1, t_2) for the integral by solving $x^2 + y^2 + z^2 = R^2$ for $x = \vartheta t$, $y = t - d$, $z = \varphi t$ for t . Here is R the radius (edge) of the galaxy cluster.

2.2 Optical depth

As previously stated, the equation (1.5) can calculate the optical depth. Solving this equation for all angles φ and ϑ in direction of the galaxy cluster using definition (2.2) with parametrization (2.1) leads to figure 2.3. The angles were transformed to the radius of the galaxy cluster in units of the core radius. For the electron density, equation (1.7), are the median values in Baldi et al. (2018) [9] used.

$$r_c = 0.2 \text{ Mpc}, r_s = 1.7 \text{ Mpc}, n_0 = 2 \times 10^4 \text{ m}^{-3}, \alpha = 1, \beta = 0.7, \epsilon = 2.5 \quad (2.4)$$

The Thomson cross-section for electrons is $\sigma_T = 6.652 \times 10^{-29} \text{ cm}^2$ [20]. These parameters are used for all further calculations.

As one would expect, the optical depth is greatest in the direction of the center. This stems from the fact that, on the one hand, the electron density is greatest there and on the other hand, the line of sight through the cluster is longest. The sudden drop at the edge is caused by the hard definition of the cluster size.

2.3 Rotational velocity

Owing to the little knowledge about the rotational dynamics of the ICM, I perform most calculations with the two velocity profiles introduced in section 1.2. But mainly use the profile provided in Baldi et al. (2018) [9]. Since it seems, this profile describes the rotation of galaxy clusters more realistically.

The solid-body rotation with a saturation towards the edge will later be referenced to as VP1 and can be expressed as:

$$v_{\text{VP1}}(r) = v_c \cdot \frac{r}{r_c} \quad (2.5)$$

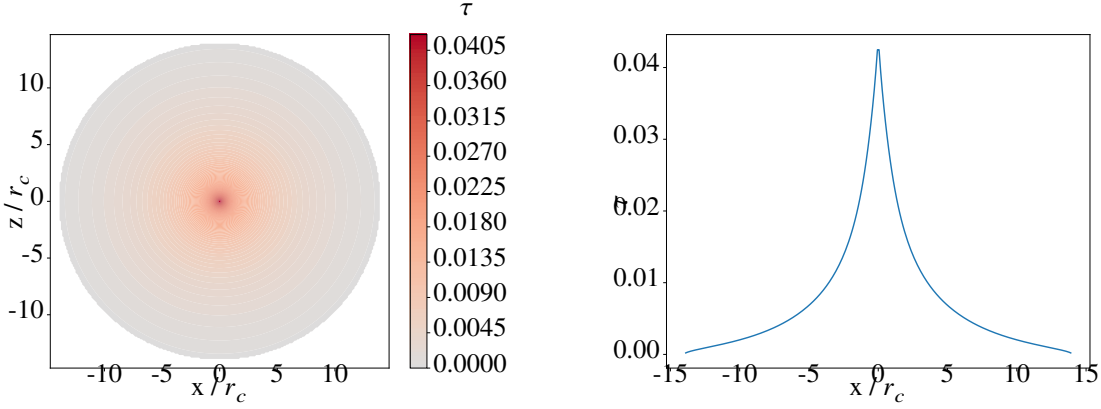


Figure 2.3: optical depth of galaxy cluster with $r_c = 0.2 \text{ Mpc}$, $R = R_{\text{vir}} = 14r_c$ and electron density (1.7) and values (2.4)

Figure 2.4: cut of optical depth profile at $z=0$ of galaxy cluster to the left, fig. 2.3

v_c is the velocity at the core radius r_c .

The second velocity profile (VP2) by [9, Baldi et al. (2018)] follows:

$$v_{\text{VP2}}(r) = v_{t0} \cdot \frac{\frac{r}{r_0}}{1 + (\frac{r}{r_0})^2} \quad (2.6)$$

r_0 is the scale radius and corresponds to the radius of the peak velocity. The scale velocity v_{t0} is double the velocity of the peak. In Baldi et al. (2018) [9] values of $r_0 \sim 1.2 \text{ Mpc}$ and $v_{t0} \sim 800 \text{ km s}^{-1}$ were found.

The characteristics of both profiles can be compared in figure 2.5. The average velocity along the radius for the used velocity profiles is about the same at $\sim 330 \text{ km s}^{-1}$

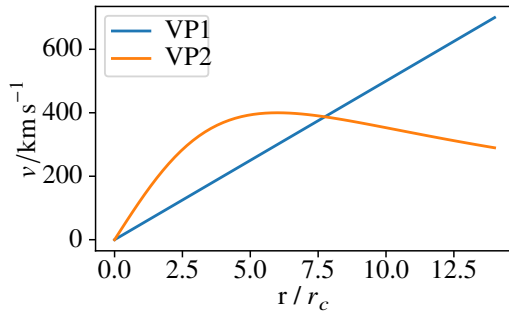


Figure 2.5: velocity profiles VP1 with $v_c = 50 \text{ km s}^{-1}$ & VP2 with $v_{t0} = 800 \text{ km s}^{-1}$ and $r_0 = 1.2 \text{ Mpc}$

Velocity profiles VP1 and VP2 can be used by multiplying with a constant velocity field:

$$\vec{v}(\vec{r}) = \begin{pmatrix} -y \\ x \\ 0 \end{pmatrix} \frac{1}{\sqrt{x^2 + y^2}} \cdot v_{VPi}(r) \quad (2.7)$$

This is a rotating vector field along the z-axis following the velocity profile i . In equation (2.5 - 2.7) is $\vec{r} = (x, y, z)^T$ and $r = \sqrt{x^2 + y^2}$, the distance from the rotation axis (z-axis).

The rotation axis can be rotated along the x- and y-axis to suit any orientation. I define the inclination $i = 0$ for the rotation along the line of sight and $i = \pi/2$ for the axis of rotation parallel to the z-axis as in equation (2.7).

Besides the parameters (2.4), I use the parameters (from Cooray and Chen (2002) [11] and mean values in Baldi et al. (2018) [9])

$$v_c = 50 \text{ km s}^{-1}, v_{t0} = 800 \text{ km s}^{-1}, r_0 = 1.2 \text{ Mpc} \quad (2.8)$$

for the velocity profiles in all following calculations.

2.4 Relative intensity change

As described in section 1.3.4, the relative intensity change of the CMB, caused by the kSZE, is independent of the velocity transversal to the observer. Therefore is $v_x = v_z = 0$. According to equation (1.8), with the optical depth equation (1.5), the relative intensity change along the line of sight then results in:

$$\frac{\Delta I_\nu}{I_\nu} = G_\nu \vec{\beta}_\parallel(\vec{l}) \sigma_T n_e(\vec{l}) d\vec{l} \quad (2.9)$$

After inserting the electron density (1.7) and rotating velocity field (2.7), one can calculate the relative intensity change using definition (2.3) and parametrization (2.1).

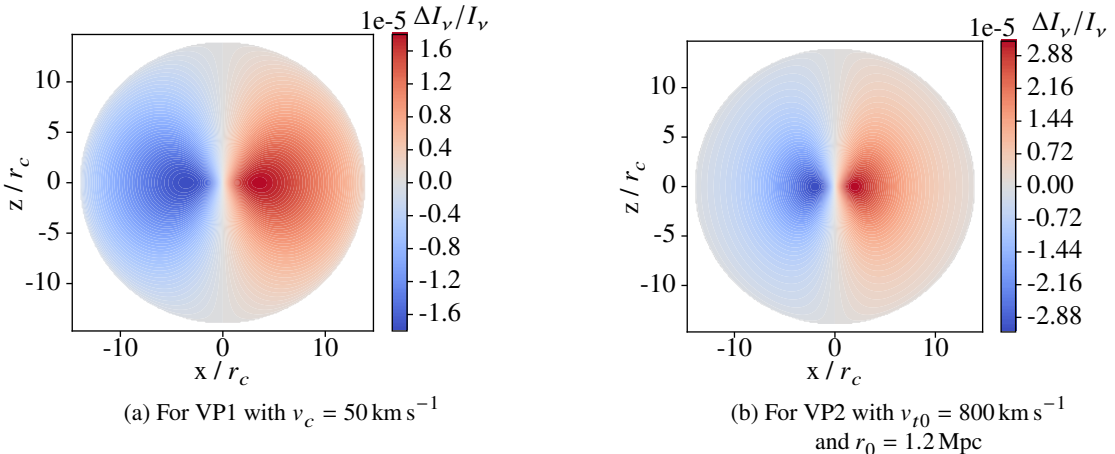


Figure 2.6: relative intensity change at the CMB intensity peak $\nu = 160 \text{ GHz}$. Galaxy cluster with $i = \pi/2$, $r_c = 0.2 \text{ Mpc}$, $R = R_{\text{vir}} = 14r_c$, electron density (1.7), and values (2.4) and (2.8)

In the center, the relative intensity change is zero because the galaxy cluster there has no movement along the line of sight, respectively it changes direction. The same applies everywhere at $z = 0$. Left and right to the center, one can see two extremes. These occur because the optical depth is the greatest there (as seen in the previous section (2.2)) and the velocity has a large parallel component to the line of sight. The dipole is caused by the fact that the cluster rotates and therefore one side moves towards and the other away from the observer. This rkSZE leads to an increase and decrease in intensity of the CMB radiation due to Thompson scattering. The sudden drop at the edge can again be explained by the hard definition of the cluster radius.

For both velocity profiles is the relative intensity change of the same magnitude, of $10^{-6} - 10^{-5}$. A higher electron density or velocity leads to greater changes. This is expected considering the dependencies in equation (2.9). The effect is greatest for $10^{-6} - 10^{-5}$ (see figure 2.6). Lowering the inclination i reduces the velocity component parallel to the line of sight and thus the overall intensity change. At $i = 0$ this velocity component vanishes completely, together with the intensity change. Though a rotation along the y-axis does not alter the intensity pattern but rotates it.

The relative intensity change for VP1 is lower than for VP2, although the average velocity of the used velocity profiles is similar. This is because of the higher velocities at the center where the optical depth is higher as well. Outwards the relative intensity change has a slower decrease for VP1 because of the higher velocities in the outskirts. For VP2, there is a steeper increase at the center with the maxima closer to the center than for VP1, followed by a rather fast decrease. The described differences can be well seen in figure 2.7. It is a normalized cut along the x-axis.

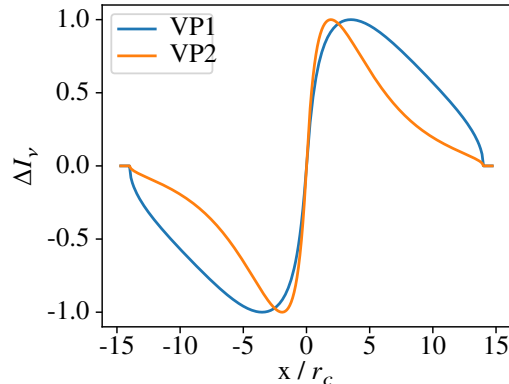


Figure 2.7: normalized cut along x-axis ($z=0$) of relative intensity change at the CMB intensity peak $\nu = 160$ GHz. Galaxy cluster with $i = \pi/2$, $r_c = 0.2$ Mpc, $R = R_{\text{vir}} = 14r_c$, electron density (1.7), and values (2.4) and (2.8)

2.4.1 Temperature change

As explained in section 1.3.4 the rkSZE can also be expressed as a change in the CMB temperature:

$$\Delta T_{\text{CMB}} = T_{\text{CMB}} \beta_{\parallel} \sigma_T n_e(\vec{l}) d\vec{l} \quad (2.10)$$

Processing this in the same way as equation (2.9) and at the CMB temperature of 2.725 K one gets a temperature change of up to a few tenth μK (see figure 2.8)

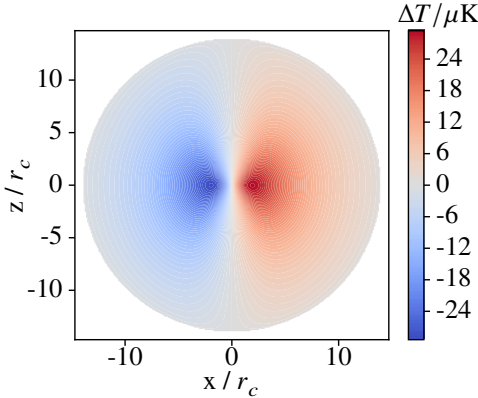


Figure 2.8: CMB temperature change. Galaxy cluster with VP2, $\mathbf{i} = \pi/2$, $r_c = 0.2$ Mpc, $R = R_{\text{vir}} = 14r_c$, electron density (1.7), and values (2.4) and (2.8)

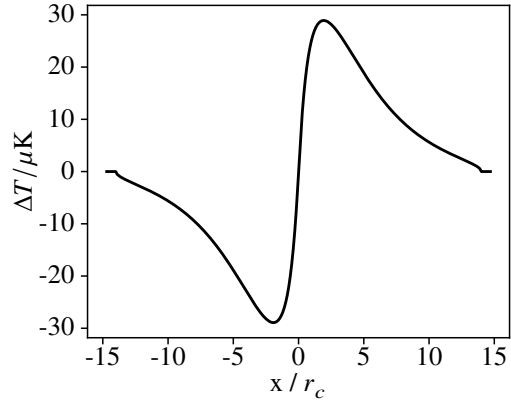


Figure 2.9: Cut along the x-axis ($z=0$) of the CMB temperature change to the left

The temperature change has the same profile and behavior as the relative intensity change. It only has another scale. The VP1 variant can be seen in the appendix (see figure 4.1 & 4.2).

2.5 Polarization

Besides the intensity change, the SZE causes polarization of the CMB (see section 1.3.5). Contrary to the intensity change, this effect depends only on the transverse motion to the observer. Thus, for further discussion, a cluster with the rotational axis parallel to the line of sight is considered. The inclination is $\mathbf{i} = 0$.

The *Sookes* parameters Q and U are calculated according to equations (1.11) and (1.12) with the optical depth (1.5) to:

$$Q = -\frac{1}{10} I_0 G_{\nu, \text{pol}} \vec{\beta}_\perp^2 \cos(2\chi) \sigma_T n_e(l) dl \quad (2.11)$$

$$U = -\frac{1}{10} I_0 G_{\nu, \text{pol}} \vec{\beta}_\perp^2 \sin(2\chi) \sigma_T n_e(l) dl \quad (2.12)$$

Since these only depend on the transverse part of the velocity is $v_y = 0$. Q and U can then be calculated using definition (2.2) and parametrization (2.1).

The linear polarization degree is calculated according to equation (1.13) with $I_{\text{tot}} \approx I_0$ because τ and I_s are small (see sections 2.2 and 2.4).

$$P = \frac{\sqrt{Q^2 + U^2}}{I_0} \quad (2.13)$$

The polarisation plane for Thompson scattering is perpendicular to the moving direction of the charged particle. As Q describes the vertical and horizontal polarization and U the 45° rotated polarization, one derives the octupole pattern because of the circular velocity of the ICM, which can be seen in figures 2.10 and 2.11. This results then in the circular uniform linear polarization degree P

(see figure 2.12).

The polarization angle in figure 2.12 is calculated by [12]:

$$2\theta = \begin{cases} \arctan\left(\frac{U}{Q}\right) & Q \geq 0 \\ \arctan\left(\frac{U}{Q}\right) + \pi & Q < 0 \end{cases} \quad (2.14)$$

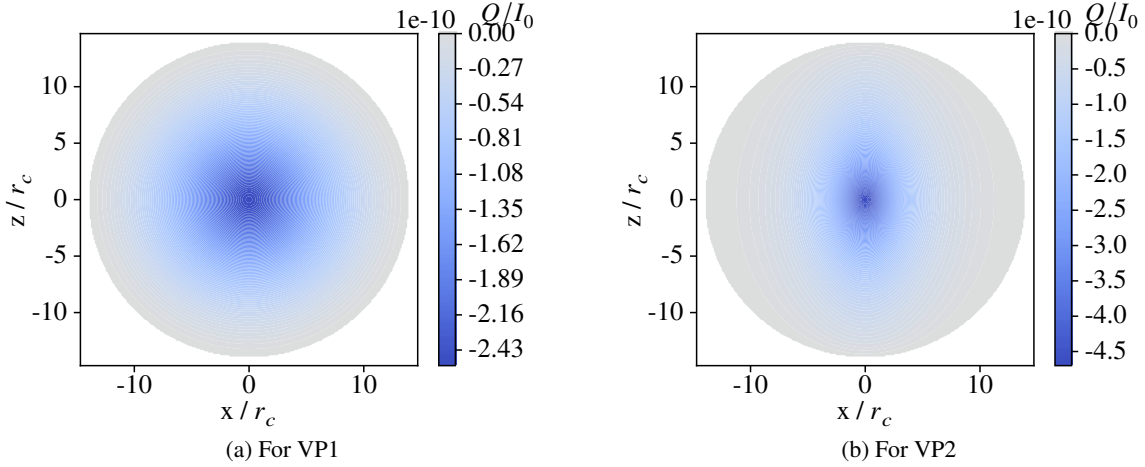


Figure 2.10: Stokes parameter Q of linear polarization. Galaxy cluster with $i = 0$, $r_c = 0.2$ Mpc, $R = R_{\text{vir}} = 14r_c$, electron density (1.7), and values (2.4) and (2.8)

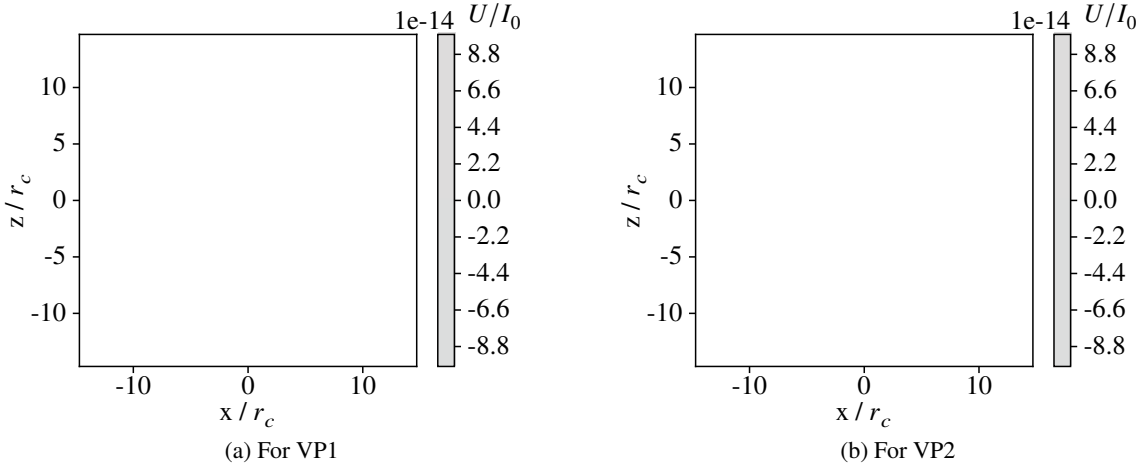


Figure 2.11: Stokes parameter U of linear polarization. Galaxy cluster with $i = 0$, $r_c = 0.2$ Mpc, $R = R_{\text{vir}} = 14r_c$, electron density (1.7), and values (2.4) and (2.8)

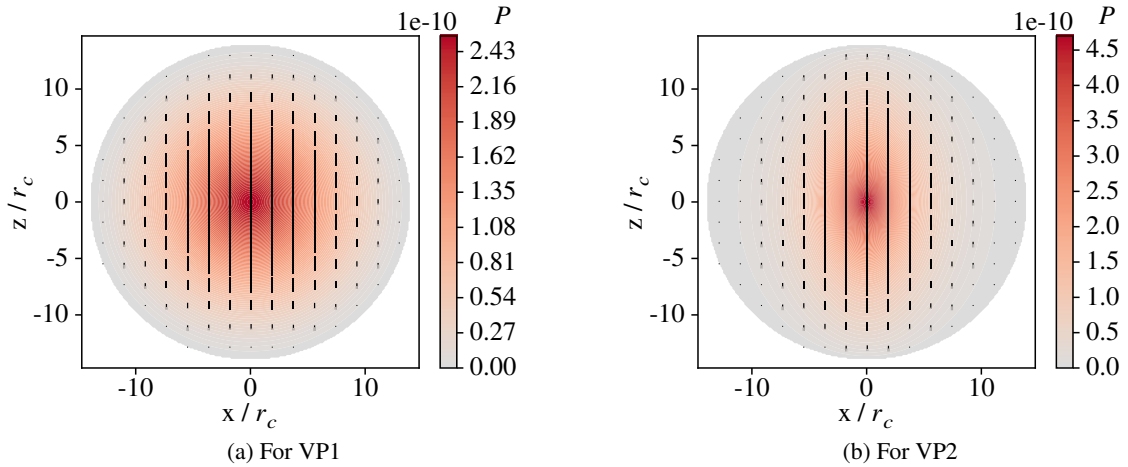


Figure 2.12: polarization degree P (color scale) and polarization planes (black lines, length proportional to P). Galaxy cluster with $i = 0, r_c = 0.2 \text{ Mpc}, R = R_{\text{vir}} = 14r_c$, electron density (1.7), and values (2.4) and (2.8)

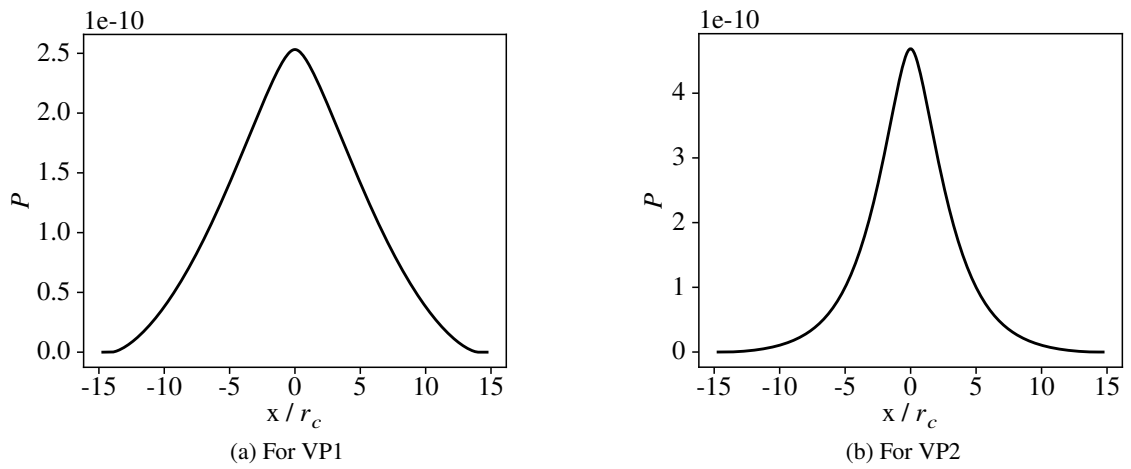


Figure 2.13: cut along x-axis ($z=0$) of polarization degree P . Galaxy cluster with $i = 0$, $r_c = 0.2 \text{ Mpc}$, $R = R_{\text{vir}} = 14r_c$, electron density (1.7), and values (2.4) and (2.8)

One can see a significant impact of the velocity profile on the polarization profiles. Comparing the Stokes parameters Q and U of VP1 and VP2 in figures 2.10 and 2.11 one can see for both the even quadrupoles, resulting in the circular uniform degree of polarization P in figure 2.12. But for VP2, the maxima are closer to the center. Figure 2.13 shows this clearly. This fits the profile of the relative intensity change (compare figure 2.7). But the maxima for the polarization are even closer to the center due to the β^2 dependency. The vanishing polarization in the center arises from the missing movement of the ICM there.

A variation of the inclination leads, for the polarization, to a stronger alteration than in the case of relative intensity change. Increasing the inclination from $i = 0$ leads to a horizontal velocity component in the center and therefore to $Q(r = 0) \neq 0$ and a third maximum in the degree of polarization P , along the x-axis, in the center (see figure 4.3(d)). Overall, the degree of polarization becomes more complex with 4 extremes arranged in a quadrupole pattern (compare figures 4.3(c) - 4.5(c)). The minimum in the center splits and propagates outwards along the x-axis. Contrary, the circular maximum becomes more significant at the z-axis, falls off towards the x-axis, encloses the minima, and propagate to the center. The radial orientation of the polarization remains but fades with a rising vertical component, as the vertical velocity component and therefore U decreases (see figures 4.3(b) - 4.5(b)), while the maxima of the Stokes parameter Q fade and the minima move together (see figures 4.3(a) - 4.5(a)).

The referenced polarisation parameters for $i = \pi/8$ are shown in the appendix section 4.3. Since the polarization profile only changes slightly in dependence upon the velocity profile, the representation for VP1 is omitted at this point.

The closer the inclination gets to $i = \pi/2$, the more the minima of the polarization degree vanish and the maxima merge in the center. A polarization degree profile similar to that of the optical depth with a maximum in the center is left. The polarization planes are now parallel to the axis of rotation (see figure 4.6). The representation for VP1 is omitted again at this point.

For all previous instances the clusters where only rotated along the x-axis, change of inclination. But not along the y-axis. A rotation along the y-axis only changes the orientation of the $Q, U \& P$ profiles, like in case of the relative intensity change.

2.5.1 Average polarization of multiple galaxy clusters

The degree of polarization is extremely small, which makes direct observation difficult. A solution to this problem could be to stack multiple polarization images of galaxy clusters. If the average stokes parameters Q and U and the degree of polarization do not vanish it could be possible to observe polarization due to the SZE. Averaging will bring down the noise level due to the stochastic nature of noise, while keeping the signal unchanged, so this will improve the signal-to-noise ratio. Even though the modelling presented in this thesis contains no noise, such averaging is a standard procedure in astronomical data analysis.

To investigate this, have first a look at galaxy clusters with $i = \pi/2$ and a random rotation along the y-axis. This leads to a disappearance of polarization, since the polarization orientation always points in a random direction and two polarization planes rotated by 90° cancel each other out.

Galaxy clusters with $i \neq \pi/2$ always have at least a small radial polarization orientation component. This component always points in the same direction and therefore does not vanish.

Considering these two effects, one would expect that the polarization component provided by the inclination $i \neq 0$, causing the central maximum (e.g. in figure 4.4(d)) to vanish and only the radial

polarization component is left over, for multiple stacked clusters. This results in a polarization similar to that of a single galaxy cluster with $i = 0$.

To verify this statement the average Stokes parameters Q and U of 100 galaxy clusters with random inclinations and rotation angles along the line of sight (y-axis) were calculated. As before, the calculation for VP1 is omitted. The resulting polarization parameters are shown in figure 2.14. The profiles of the Stokes parameters and the degree of polarization are similar to the results determined for a single galaxy cluster with $i = 0$ and fulfil our expectations. If one takes a closer look at the center, one can still see residual minima similar to a cluster with e.g. $i = \pi/8$ (see figure 4.3(c)). Increasing the stacked galaxy clusters shifts these maxima further into the center. Until they merge for an infinite number of clusters at $r=0$. This tendency can be seen in figure 4.7. There 1000 galaxy clusters were stacked. With the resolution of the calculation no quadrupole is recognisable.

In addition to the divergent inclination, this method can be used to even out irregularities in the rotation pattern of individual clusters. Enabling the investigation of the fundamental rotational dynamics of galaxy cluster.

In case of the relative intensity change the stacking procedure is not possible, since there is only a dipole and no circular symmetry. Consequently the relative intensity change vanishes for random rotation orientations.

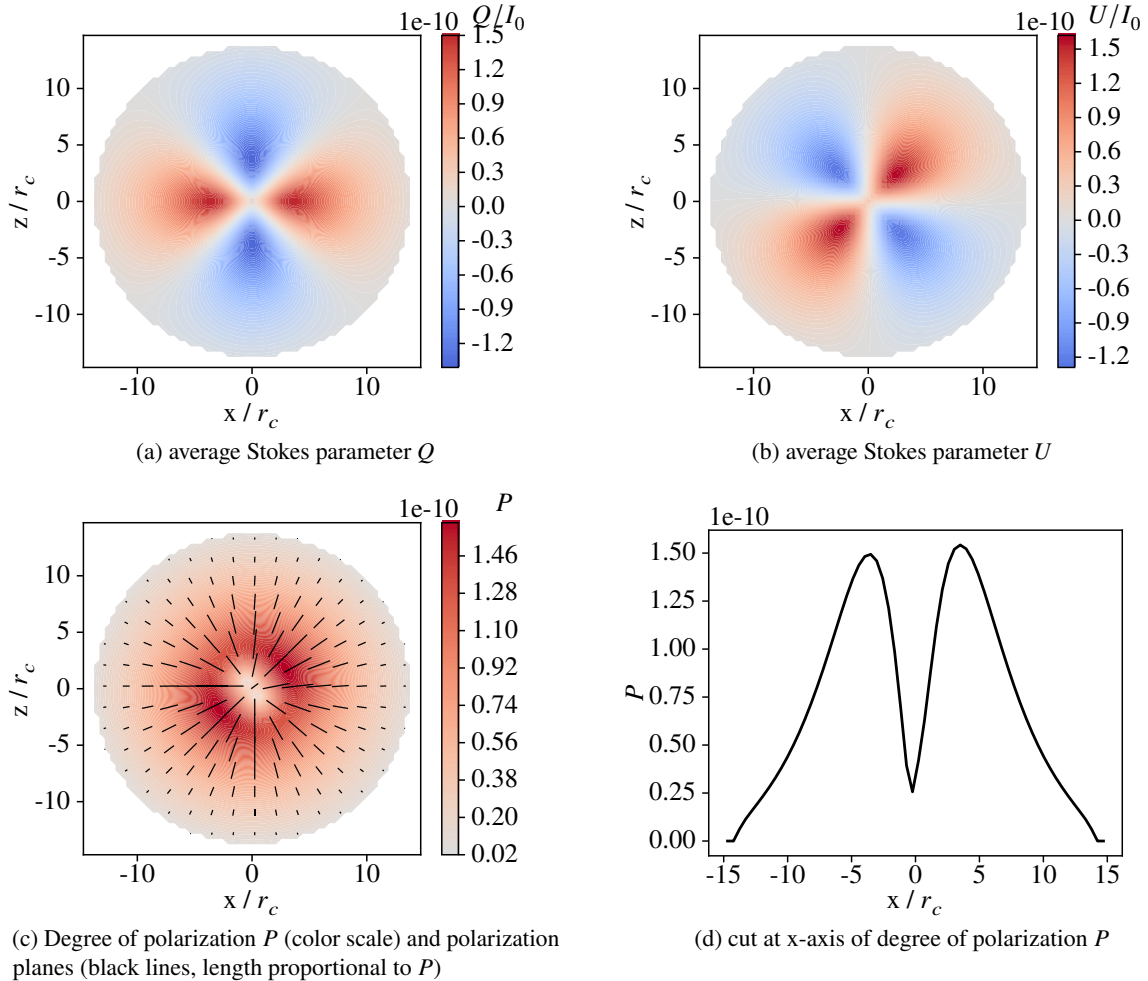


Figure 2.14: average Stokes parameters and degree of polarization of 100 stacked galaxy clusters with random orientation of rotation axis, $r_c = 0.2$ Mpc, $R = R_{\text{vir}} = 14r_c$, electron density (1.7), and values (2.4)

CHAPTER 3

Conclusion and Outlook

In this thesis, the kinetic Sunyaev-Zeldovich effect and the polarizing effect of the CMB by scattering of ICM electrons were examined.

The relative intensity change by the kSZE was simulated for two rotational velocity profiles of galaxy clusters and then compared. The resulting dipoles were found to be similar with slight differences in strength of the distortion and slope of the profile. For the peak intensity of the CMB ($\nu = 160$ GHz) was a relative intensity change of the order $10^{-6} - 10^{-5}$ found. The same effect can be described as a shift in the CMB temperature. It was determined to be up to about $30 \mu\text{K}$. These finding are in agreement with the results in Chluba and Mannheim (2002) [12] and Baldi et al. (2018) [9].

The polarization of the CMB radiation was simulated for several inclinations of the rotation axis. For the rotation axis parallel to the line of sight, the polarization was found to have a radial direction. The degree of polarization was found to be very small, too small to be observed directly. It is of the order of $10^{-11} - 10^{-10}$.

It was also investigated whether polarization remains after stacking multiple clusters with random rotational orientations. The average Stokes parameters Q and U were found not to vanish. They do, however, take the rudimentary form for a single galaxy cluster where the rotation axis is parallel to the line of sight. This behavior can be a useful tool to better understand the rotational dynamics of galaxy clusters.

With the right tools, the result of stacked galaxy clusters could be measured and thus could be highly useful for studying the rotational dynamics of galaxy clusters. One must find out if the core radius is a good fit as the unit of scale, or if there is another, better scale radius so the polarization sums up well. Perhaps the scale radius r_0 of the velocity profile VP2 is a better fit or even the virial radius R_{vir} , as used in Baldi et al. (2018) [9]. Another question is whether the velocity profile VP2 fits at all. Or if there is an even better profile. This could be determined with this method since the velocity profile has a significant impact in the polarization degree profiles, as seen in figure 2.13.

CHAPTER 4

Appendix

4.1 Software

The software used for the calculations can be found on GitHub: <https://github.com/npaessler/Kinetic-Sunyaev-Zeldovich-effect-from-galaxy-cluster-rotation>

The software was written in `jupyter-notebook` using Python 3.10.4 – docs.python.org – and the following modules:

- `matplotlib 3.5.1` – matplotlib.org
- `numpy 1.22.3` – numpy.org
- `scipy 1.8.0` – scipy.org

4.2 Temperature change figure

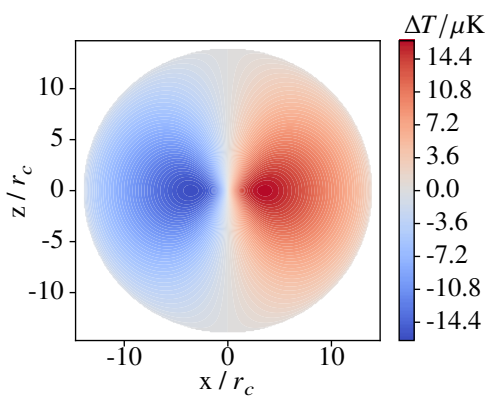


Figure 4.1: CMB temperature change. Galaxy cluster with VP1, $i = \pi/2$, $r_c = 0.2$ Mpc, $R = R_{\text{vir}} = 14r_c$, electron density (1.7), and values (2.4) and (2.8)

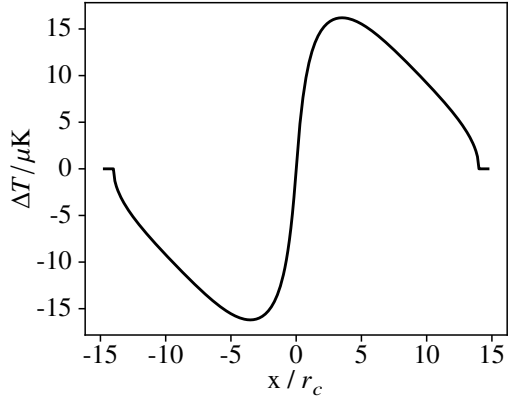


Figure 4.2: Cut along the x-axis ($z=0$) of the CMB temperature change to the left

4.3 Polarization figures

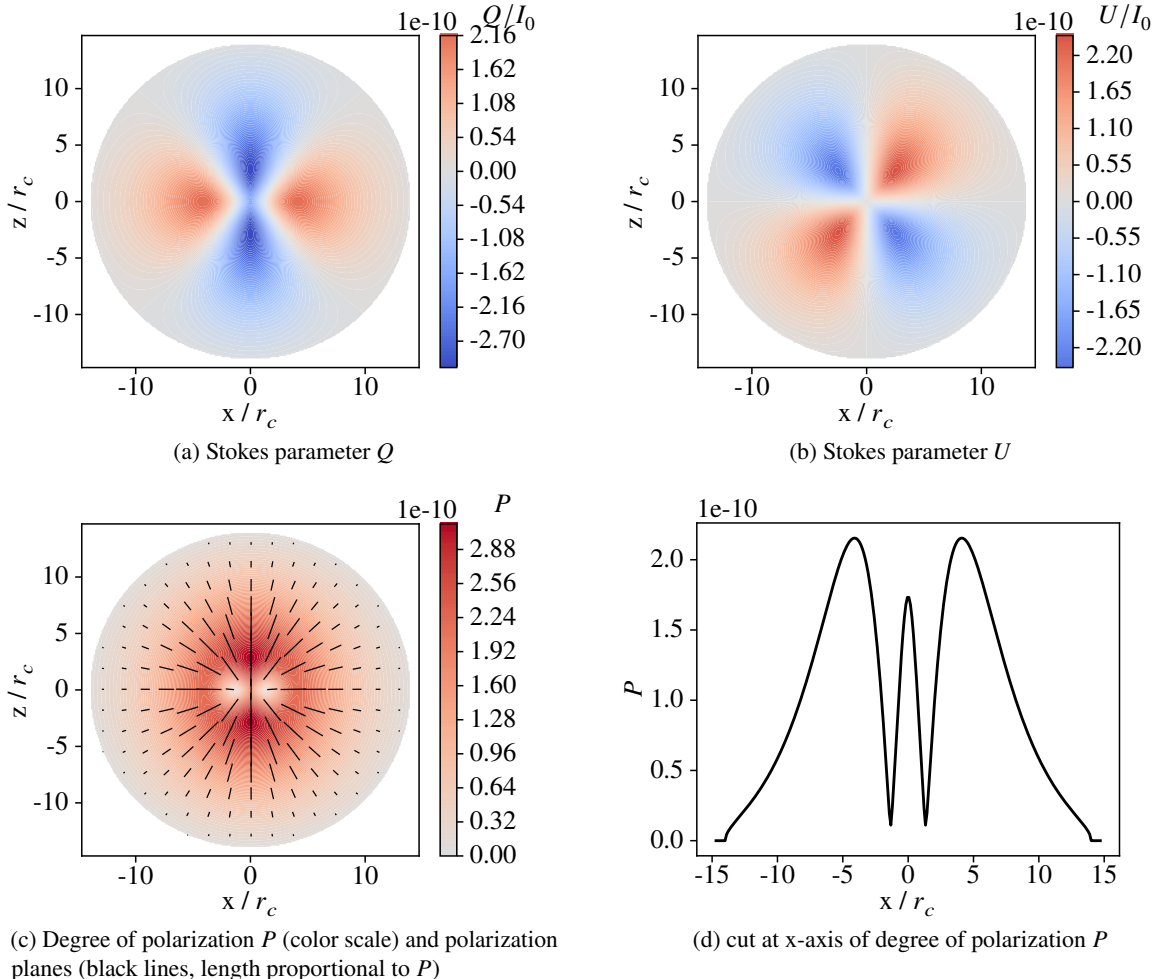


Figure 4.3: polarization parameters of linear polarization caused by rotating galaxy cluster with $i = \pi/8$, $r_c = 0.2$ Mpc, $R = R_{\text{vir}} = 2.8$ Mpc = $14r_c$, electron density (1.7) and values (2.4)

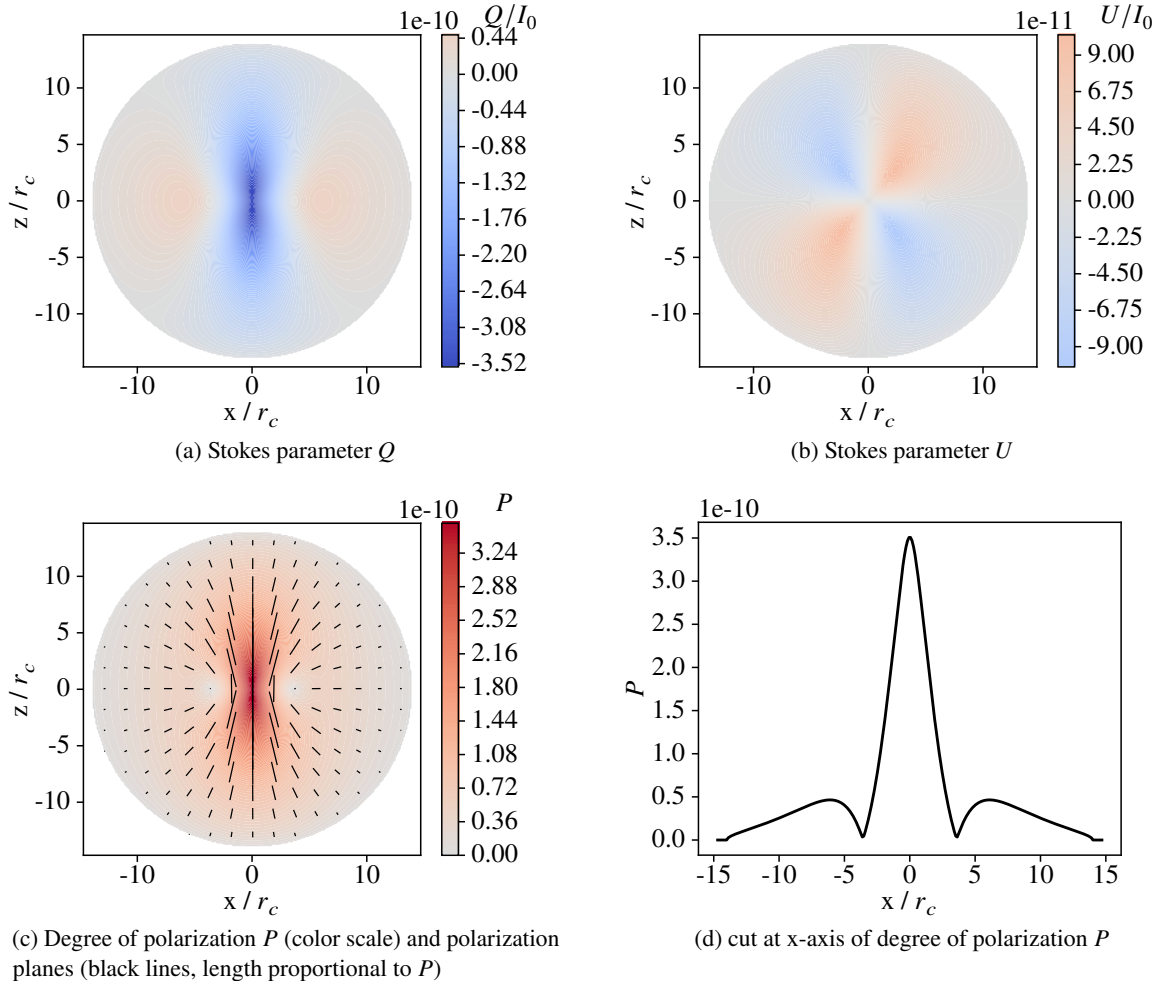


Figure 4.4: polarization parameters of linear polarization caused by rotating galaxy cluster with $i = \pi/4$, $r_c = 0.2$ Mpc, $R = R_{\text{vir}} = 2.8$ Mpc = $14r_c$, electron density (1.7) and values (2.4)

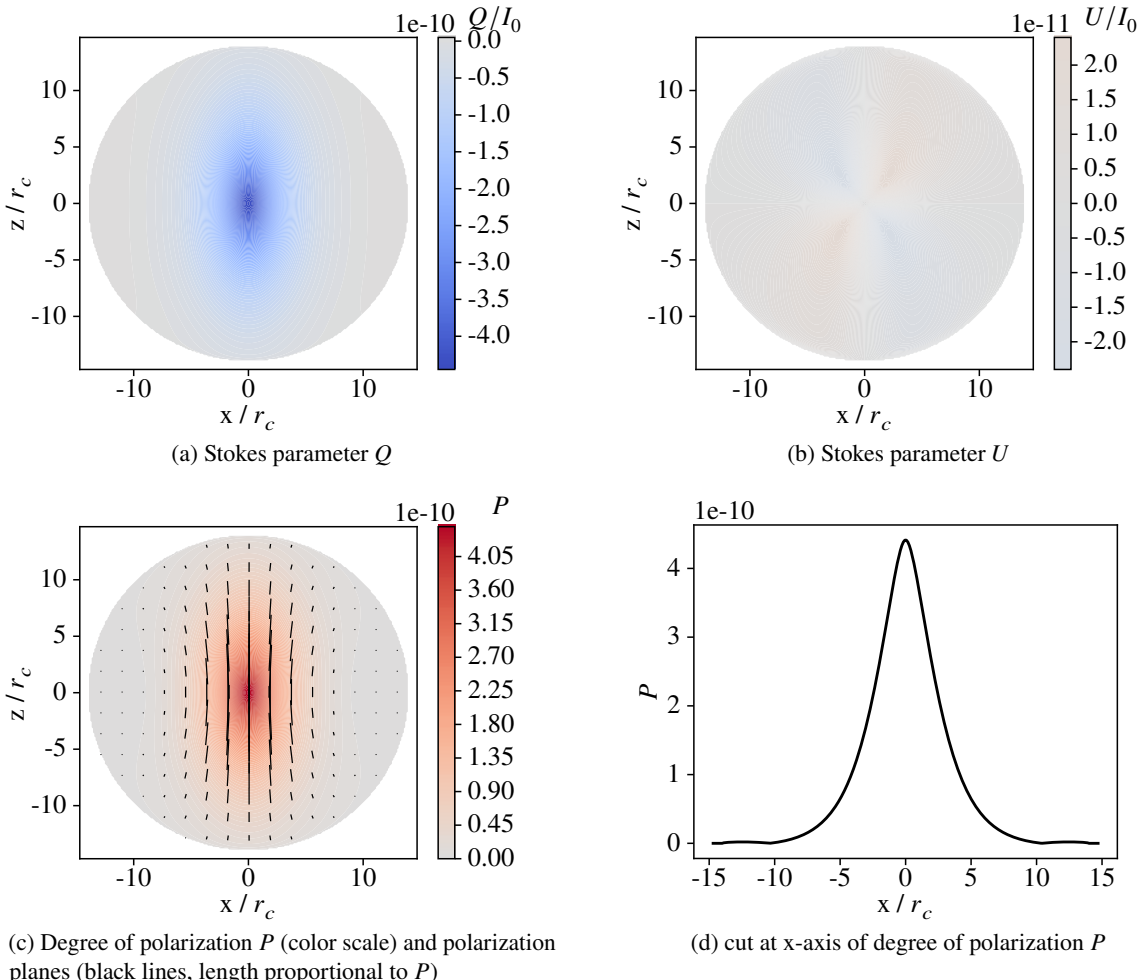


Figure 4.5: polarization parameters of linear polarization caused by rotating galaxy cluster with $i = \pi/3/8$, $r_c = 0.2$ Mpc, $R = R_{\text{vir}} = 2.8$ Mpc = $14r_c$, electron density (1.7) and values (2.4)

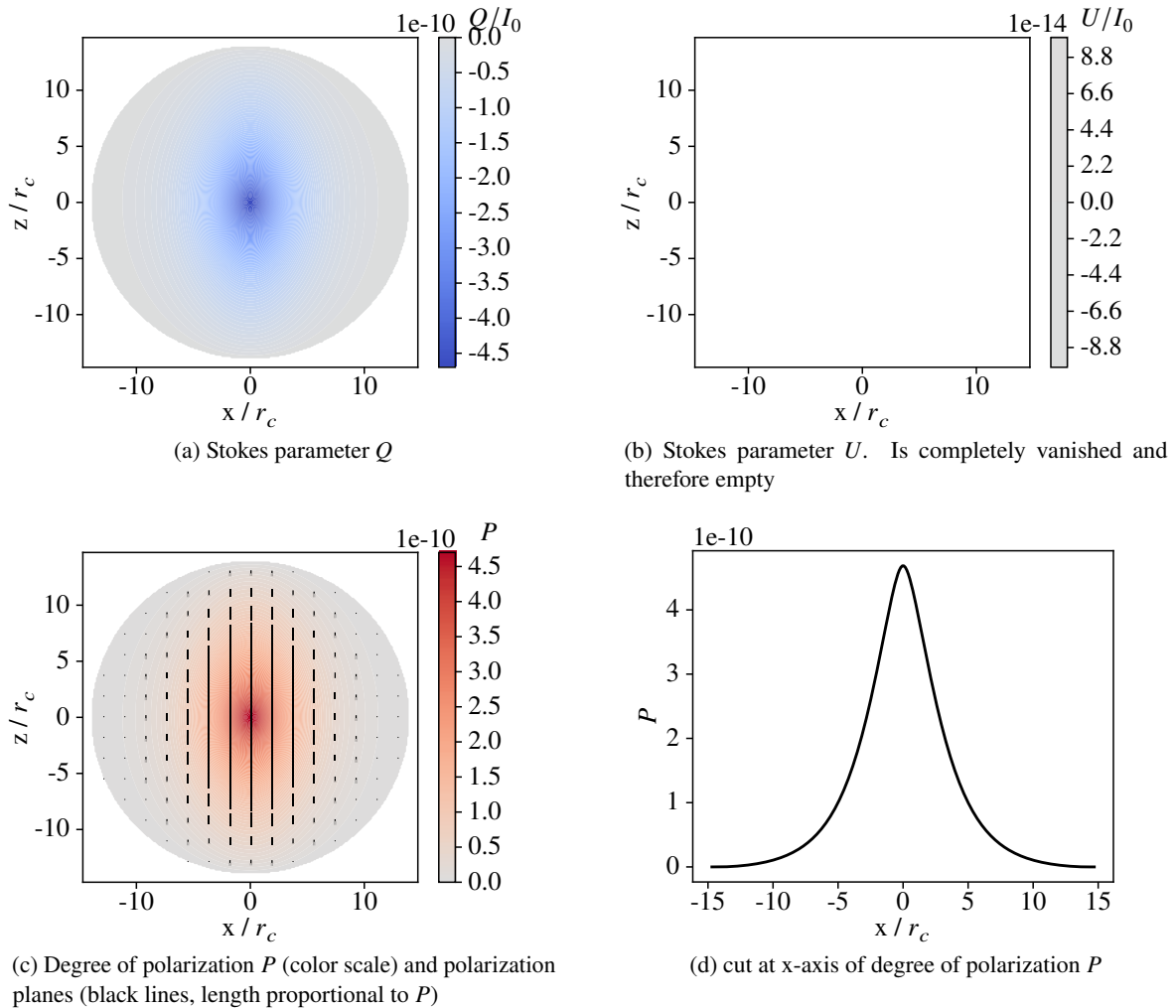


Figure 4.6: polarization parameters of linear polarization caused by rotating galaxy cluster with $i = \pi/2$, $r_c = 0.2$ Mpc, $R = R_{\text{vir}} = 2.8$ Mpc = $14r_c$, electron density (1.7) and values (2.4)

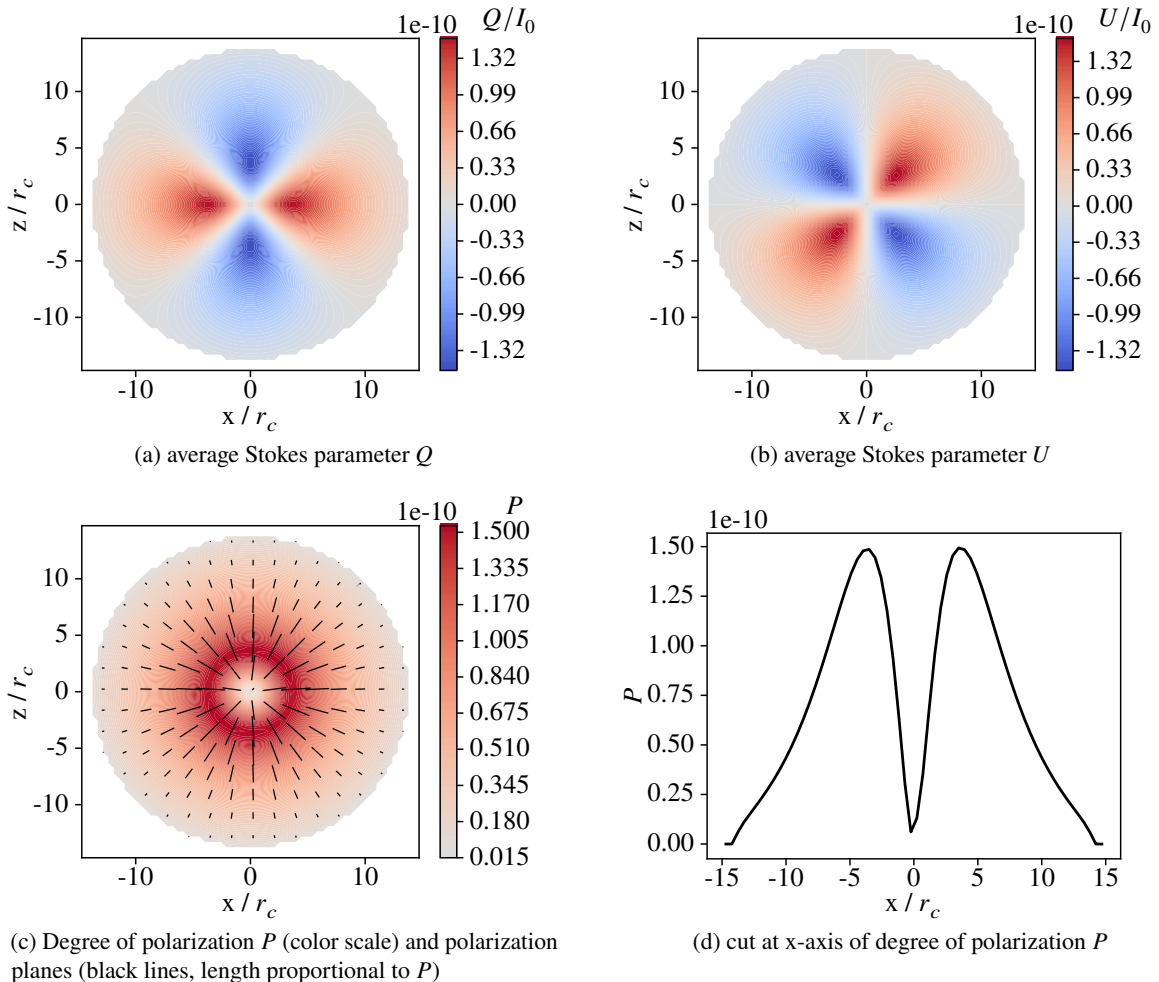


Figure 4.7: average Stokes parameters and degree of polarization of 1000 stacked galaxy clusters with random orientation of rotation axis, $r_c = 0.2$ Mpc, $R = R_{\text{vir}} = 14r_c$, electron density (1.7), and values (2.4)

Bibliography

- [1] *Anisotropies in the CMB*, 1999, arXiv: [astro-ph/9903232 \[astro-ph\]](#).
- [2] N. Aghanim et al., *Planck2018 results, Astronomy & Astrophysics* **641** (2020) A1, issn: 1432-0746, URL: <http://dx.doi.org/10.1051/0004-6361/201833880>.
- [3] D. Scott, *The standard cosmological model*, Canadian Journal of Physics **84** (2006) 419, issn: 1208-6045, URL: <http://dx.doi.org/10.1139/P06-066>.
- [4] S. Chandrasekhar, *Radiative transfer*, 1960.
- [5] A. N. Cox, *Allen's astrophysical quantities*, 2000.
- [6] N. A. Bahcall, *Core radii and central densities of 15 rich clusters of galaxies.*, **198** (1975) 249.
- [7] M. Arnaud, *The β -model of the intracluster medium. Commentary on: Cavaliere A. and Fusco-Femiano R.*, 1976, *A&A*, 49, 137, *Astronomy & Astrophysics* **500** (2009) 103.
- [8] A. Vikhlinin et al., *Chandra Sample of Nearby Relaxed Galaxy Clusters: Mass, Gas Fraction, and Mass-Temperature Relation*, *The Astrophysical Journal* **640** (2006) 691, URL: <https://doi.org/10.1086/500288>.
- [9] A. S. Baldi et al., *Kinetic Sunyaev–Zel'dovich effect in rotating galaxy clusters from MUSIC simulations*, *Monthly Notices of the Royal Astronomical Society* **479** (2018) 4028, URL: <https://doi.org/10.1093/mnras/sty1722>.
- [10] F. Sembolini et al., *The MUSIC of galaxy clusters – I. Baryon properties and scaling relations of the thermal Sunyaev–Zel'dovich effect*, *Monthly Notices of the Royal Astronomical Society* **429** (2012) 323, issn: 0035-8711, eprint: <https://academic.oup.com/mnras/article-pdf/429/1/323/3345321/sts339.pdf>, URL: <https://doi.org/10.1093/mnras/sts339>.
- [11] A. Cooray and X. Chen, *Kinetic Sunyaev-Zeldovich Effect from Halo Rotation*, *The Astrophysical Journal* **573** (2002) 43, issn: 1538-4357, URL: <http://dx.doi.org/10.1086/340582>.
- [12] J. Chluba and K. Mannheim, *Kinetic Sunyaev-Zeldovich effect from galaxy cluster rotation*, *Astronomy & Astrophysics* **396** (2002) 419, issn: 1432-0746, URL: <http://dx.doi.org/10.1051/0004-6361:20021429>.

Bibliography

- [13] A. S. Baldi et al.,
On the coherent rotation of diffuse matter in numerical simulations of clusters of galaxies,
Monthly Notices of the Royal Astronomical Society **465** (2016) 2584, ISSN: 0035-8711,
eprint: <https://academic.oup.com/mnras/article-pdf/465/3/2584/8420148/stw2858.pdf>,
URL: <https://doi.org/10.1093/mnras/stw2858>.
- [14] Y. B. Zeldovich and R. A. Sunyaev,
The Interaction of Matter and Radiation in a Hot-Model Universe, **4** (1969) 301.
- [15] R. A. Sunyaev and Y. B. Zeldovich, *The velocity of clusters of galaxies relative to the microwave background - The possibility of its measurement.*,
Monthly Notices of the Royal Astronomical Society **190** (1980) 413.
- [16] S. Y. Sazonov and R. A. Sunyaev, *Microwave polarization in the direction of galaxy clusters induced by the CMB quadrupole anisotropy*,
Monthly Notices of the Royal Astronomical Society **310** (1999) 765, ISSN: 1365-2966,
URL: <http://dx.doi.org/10.1046/j.1365-8711.1999.02981.x>.
- [17] G. Lavaux, J. M. Diego, H. Mathis and J. Silk,
Sunyaev-Zel'dovich polarization as a probe of the intracluster medium,
Monthly Notices of the Royal Astronomical Society **347** (2004) 729, ISSN: 1365-2966,
URL: <http://dx.doi.org/10.1111/j.1365-2966.2004.07265.x>.
- [18] I. Khabibullin, S. Komarov, E. Churazov and A. Schekochihin, *Polarization of Sunyaev–Zel’dovich signal due to electron pressure anisotropy in galaxy clusters*,
Monthly Notices of the Royal Astronomical Society **474** (2017) 2389, ISSN: 0035-8711,
eprint: <https://academic.oup.com/mnras/article-pdf/474/2/2389/22731247/stx2924.pdf>,
URL: <https://doi.org/10.1093/mnras/stx2924>.
- [19] “Linienintegrale”, *Mathematik 1: Geschrieben für Physiker*,
Berlin, Heidelberg: Springer Berlin Heidelberg, 2005 343, ISBN: 978-3-540-26652-5,
URL: https://doi.org/10.1007/3-540-26652-6_16.
- [20] E. Tiesinga, P. Mohr, D. Newell and B. Taylor,
CODATA Recommended Values of the Fundamental Physical Constants: 2018, en, (2021),
URL: https://tsapps.nist.gov/publication/get_pdf.cfm?pub_id=931443.

List of Figures

2.1	Coordinate system	8
2.2	Line of sight parametrization	8
2.3	optical depth of galaxy cluster with $r_c = 0.2 \text{ Mpc}$, $R = R_{\text{vir}} = 14r_c$ and electron density (1.7) and values (2.4)	9
2.4	cut of optical depth profile at $z=0$ of galaxy cluster to the left, fig. 2.3	9
2.5	velocity profiles VP1 with $v_c = 50 \text{ km s}^{-1}$ & VP2 with $v_{t0} = 800 \text{ km s}^{-1}$ and $r_0 = 1.2 \text{ Mpc}$	9
2.6	relative intensity change at the CMB intensity peak $\nu = 160 \text{ GHz}$. Galaxy cluster with $i = \pi/2$, $r_c = 0.2 \text{ Mpc}$, $R = R_{\text{vir}} = 14r_c$, electron density (1.7), and values (2.4) and (2.8)	10
2.7	normalized cut along x-axis ($z=0$) of relative intensity change at the CMB intensity peak $\nu = 160 \text{ GHz}$. Galaxy cluster with $i = \pi/2$, $r_c = 0.2 \text{ Mpc}$, $R = R_{\text{vir}} = 14r_c$, electron density (1.7), and values (2.4) and (2.8)	11
2.8	CMB temperature change. Galaxy cluster with VP2, $i = \pi/2$, $r_c = 0.2 \text{ Mpc}$, $R = R_{\text{vir}} = 14r_c$, electron density (1.7), and values (2.4) and (2.8)	12
2.9	Cut along the x-axis ($z=0$) of the CMB temperature change to the left	12
2.10	Stokes parameter Q of linear polarization. Galaxy cluster with $i = 0$, $r_c = 0.2 \text{ Mpc}$, $R = R_{\text{vir}} = 14r_c$, electron density (1.7), and values (2.4) and (2.8)	13
2.11	Stokes parameter U of linear polarization. Galaxy cluster with $i = 0$, $r_c = 0.2 \text{ Mpc}$, $R = R_{\text{vir}} = 14r_c$, electron density (1.7), and values (2.4) and (2.8)	13
2.12	polarization degree P (color scale) and polarization planes (black lines, length proportional to P). Galaxy cluster with $i = 0$, $r_c = 0.2 \text{ Mpc}$, $R = R_{\text{vir}} = 14r_c$, electron density (1.7), and values (2.4) and (2.8)	14
2.13	cut along x-axis ($z=0$) of polarization degree P . Galaxy cluster with $i = 0$, $r_c = 0.2 \text{ Mpc}$, $R = R_{\text{vir}} = 14r_c$, electron density (1.7), and values (2.4) and (2.8)	14
2.14	average Stokes parameters and degree of polarization of 100 stacked galaxy clusters with random orientation of rotation axis, $r_c = 0.2 \text{ Mpc}$, $R = R_{\text{vir}} = 14r_c$, electron density (1.7), and values (2.4)	17
4.1	CMB temperature change. Galaxy cluster with VP1, $i = \pi/2$, $r_c = 0.2 \text{ Mpc}$, $R = R_{\text{vir}} = 14r_c$, electron density (1.7), and values (2.4) and (2.8)	21
4.2	Cut along the x-axis ($z=0$) of the CMB temperature change to the left	21
4.3	polarization parameters of linear polarization caused by rotating galaxy cluster with $i = \pi/8$, $r_c = 0.2 \text{ Mpc}$, $R = R_{\text{vir}} = 2.8 \text{ Mpc} = 14r_c$, electron density (1.7) and values (2.4)	22

List of Figures

4.4	polarization parameters of linear polarization caused by rotating galaxy cluster with $i = \pi/4, r_c = 0.2 \text{ Mpc}, R = R_{\text{vir}} = 2.8 \text{ Mpc} = 14r_c$, electron density (1.7) and values (2.4)	23
4.5	polarization parameters of linear polarization caused by rotating galaxy cluster with $i = \pi/3/8, r_c = 0.2 \text{ Mpc}, R = R_{\text{vir}} = 2.8 \text{ Mpc} = 14r_c$, electron density (1.7) and values (2.4)	24
4.6	polarization parameters of linear polarization caused by rotating galaxy cluster with $i = \pi/2, r_c = 0.2 \text{ Mpc}, R = R_{\text{vir}} = 2.8 \text{ Mpc} = 14r_c$, electron density (1.7) and values (2.4)	25
4.7	average Stokes parameters and degree of polarization of 1000 stacked galaxy clusters with random orientation of rotation axis, $r_c = 0.2 \text{ Mpc}, R = R_{\text{vir}} = 14r_c$, electron density (1.7), and values (2.4)	26